AIAA JOURNAL
Vol. 30, No. 6, June 1992

Finite Element/Penalty Function Method for Computing Stresses near Debonds

Joseph P. Fuehne*
Cooper Oil Tool Division, Houston, Texas 77251
and
John J. Engblom†
Florida Institute of Technology, Melbourne, Florida 32901

A shear deformable, finite element penalty formulation is developed for predicting stress fields, particularly interlaminar shear and normal stresses, in thick composite laminates and near a delaminated free edge in a laminated plate. A fully three-dimensional 20-noded finite element is coupled with the feature of integrating the equilibrium equations to compute interlaminar shear stresses and characterize three-dimensional stress fields. As an alternative to using the constitutive equations, the integration of the equilibrium equations provides an improved variation of interlaminar shear stresses through the thickness. Penalty functions are utilized in the formulation to represent continuity or discontinuity between layers of elements. Proficient use of these penalty functions allows simple definition of critical interfaces in a composite laminate where delamination has occurred. The flexibility of the formulation permits the consideration of different sizes of debonds without having to create a new model. In this paper, thick composite laminates are considered to demonstrate the improved variation of interlaminar shear stresses computed by integrating the equilibrium equations. Finally, a [0 deg/90 deg/0 deg] undelaminated plate subjected to uniform axial extension is compared with the same geometry containing a free-edge debond, one ply thickness in depth.

I. Introduction

DESIGN and, in particular, stress analysis of laminated composite structures are typically complex due to the orthotropy of composite materials. Closed-form or exact solutions exist only for problems that contain simple layups, boundary, and loading conditions. As a result, numerical modeling techniques derived from energy principles have assumed a large role in stress analysis of fiber-reinforced composites. Specifically, the finite element method (FEM) adapts well to problems of complex geometry, constraint, and loading conditions.

As a result of the low interlaminar strength properties of fiber-reinforced composites, characterizing interlaminar shear and normal stresses is critical and presents a challenging problem to the stress analyst. Monolithic materials do not exhibit these unique properties. The results presented herein combine research in shear deformable finite element formulations and the use of penalty functions to extend these formulations.

The shear deformable finite element formulations described by Engblom et al.,[1] which are applicable to thin to moderately thick structures, utilize a feature developed by Engblom and Ochoa[2] to compute interlaminar shear and normal stresses by integrating the equilibrium equations through the thickness. Typically, this feature results in a much-improved variation of interlaminar shear and normal stresses compared to those calculated from the constitutive equations.

Additionally, the penalty function has recently been used to extend the shear deformable finite element plate formulation whereby elements are layered through the thickness.[3,4] Penalty functions provide continuity through the thickness at interelement boundaries. Effectively, the penalty functions act as very stiff springs connecting two elements through the thickness, and the penalty parameters represent the spring constants. If the penalty parameters are set equal to a very large number, continuity is maintained; on the other hand, if the penalty parameters are set equal to zero, then a discontinuity between the two elements is modeled. Because of the versatility of the shear deformable penalty formulation, problems such as stresses in thick plates or stresses in the vicinity of debond may be studied by using the 20-noded solid element formulation.

It is notable that, in the present work, LaGrange multipliers could be used to enforce continuity between the elements. The penalty function was chosen for this purpose because it does not add degrees of freedom to the system, whereas each LaGrange multiplier represents an additional degree of freedom. Chatterjee and Ramnath[5] have used the LaGrange multiplier in their efforts to model laminated structures as an assemblage of sublaminates. In this case, a sublaminate, by their definition, is equivalent to one layer of elements in the proposed work. Although Chatterjee and Ramnath do not consider

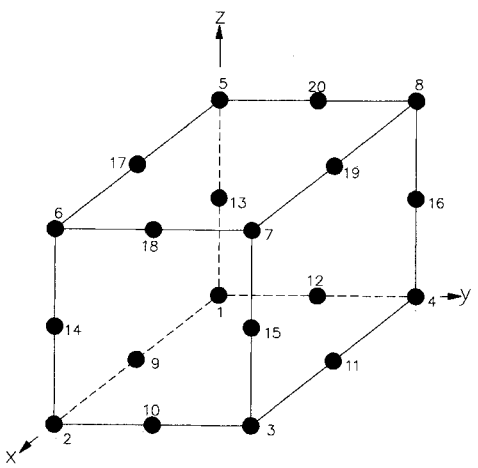

Fig. 1 Typical solid element showing nodes 1–20 and the elemental coordinate system.

Received Feb. 14, 1991; presented as Paper 91-1203 at the 32nd AIAA/ASME/ASCE/AHS/ASC Structures, Structural Dynamics, and Materials Conference, Baltimore, MD, April 8–10, 1991; revision received Aug. 23, 1991; accepted for publication Sept. 10, 1991.

*Engineering Stress Analyst, P. O. Box 1212. Member AIAA.
†Professor, Department of Mechanical and Aerospace Engineering.

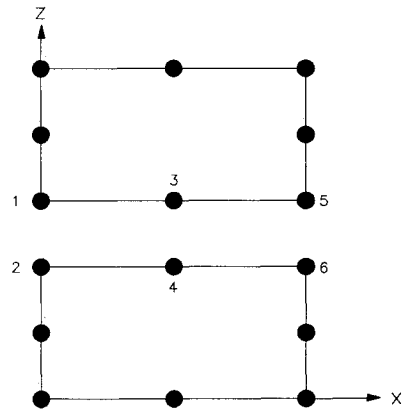

Fig. 2 Two stacked 20-noded solid elements showing nodes at the common boundary.

thick plates and shells, they do study laminated plates with delaminations.[6]

II. Displacement Variation

Engblom and Fuehne[3,4] have demonstrated the effectiveness of coupling the penalty functions and the integration of the equilibrium equations within a shear deformable plate formulation for computing interlaminar shear stresses in thick composite plates. Comparisons with elasticity solutions for problems of sinusoidal and cylindrical bending illustrate significant improvement as the number of layers is increased. However, the eight-noded plate element is inadequate in modeling problems where the interlaminar normal stress is important because the transverse displacement is assumed constant through the thickness of the element.

In order to effectively model problems that contain significant variations in interlaminar normal stress through the thickness, a 20-noded solid formulation is considered. Of particular interest is the unique coupling of the solid element formulation and the integration of the equilibrium equations to obtain interlaminar stress predictions. As a result of the transverse displacement being a function of the through the thickness coordinate, it is expected that the integration of the equilibrium equations will be effective in modeling the free-edge problem. Additionally, the penalty functions are also included in the formulation so that problems with discontinuities, like the double cantilever beam or a laminated plate with a debond at the free edge, may also be investigated.

The formulation of the 20-noded solid element is similar to that described by Cook.[7] Figure 1 shows a typical solid element with the elemental coordinate system. Each of the 20 nodes contains three displacements, but rotations are omitted. The displacements in the x, y, and z directions, in terms of nodal displacements and shape functions, are given by

$$u(x,y,z) = \sum_{i=1}^{20} N_i(\xi,\eta,\zeta)u_i \tag{1}$$

$$v(x,y,z) = \sum_{i=1}^{20} N_i(\xi,\eta,\zeta)v_i \tag{2}$$

$$w(x,y,z) = \sum_{i=1}^{20} N_i(\xi,\eta,\zeta)w_i \tag{3}$$

Utilizing these shape functions guarantees a tri-quadratic variance of displacements for the solid element. For example,

$$u = u(1,x,y,z,xy,xz,yz,xyz,\ldots,x^2,yz,xy^2z,xyz^2) \tag{4}$$

The calculation of the solid stiffness matrix uses a layer-by-layer approach that is capable of handling orthotropic plates with different fiber orientations or different materials for each layer. Evaluation of the stiffness matrix is performed by integrating over the volume of the element and using a procedure similar to the trapezoidal rule:

$$[K] = \sum_{K=1}^{NL}\left(\int_{-1}^{+1}\int_{-1}^{+1}[B]^{kT}[D]^k[B]^k\|J\|^k\,d\xi\,d\eta\right) \tag{5}$$

where NL is the number of layers in the element. It should be noted that as the summation proceeds from layer to layer, matrices $[B]$ and $[J]$ are calculated for each layer and the matrix of material properties $[D]$ is modified based on fiber orientation. The above integral is evaluated using 3×3 Gauss quadrature for all strain energy components—no shear locking effects are evident with the solid element. An eigenvalue/eigenvector test for this specialized integration scheme produced the desired six zero eigenvalues, and the associated eigenvectors accurately represent the six rigid-body modes of behavior.

Constraint Equations

Writing the constraint equations for the solid element is quite simple. Figure 2 shows two stacked 20-noded solid elements. Since the solid element has nodes that lie on the interface between the elements, the constraint equations for nodes 1 and 2 in Fig. 2 are

$$u_1 - u_2 = 0 \tag{6}$$

$$v_1 - v_2 = 0 \tag{7}$$

$$w_1 - w_2 = 0 \tag{8}$$

or, in matrix form,

$$[C]\{\delta\} = 0 \tag{9}$$

where $[C]$ is a matrix of constants, and δ is a vector of degrees of freedom.

Implementing the penalty functions to provide the constraints is quite simple. The energy functional is modified with

$$\Pi^* = \tfrac{1}{2}\{\delta\}^T[K]\{\delta\} - \{\delta\}^T\{R\} + \tfrac{1}{2}[C]^T\{\delta\}^T[\alpha][C]\{\delta\} \tag{10}$$

and minimizing gives

$$\frac{\partial\Pi^*}{\partial\delta} = \Big[[K] + [C]^T[\alpha][C]\Big]\{\delta\} - \{R\} = 0 \tag{11}$$

As a result of the penalty functions, the stiffness matrix of the finite element method is augmented by the matrix product $[C]^T[\alpha][C]$. The α term represents the penalty parameters. If $\alpha = 0$, then the constraints are ignored; however, as α grows in magnitude, the constraints are more nearly satisfied. The advantages of the penalty functions are that there are no extra degrees of freedom added to the system, which is not the case with LaGrange multipliers, and the forces of constraint between nodes, which are equivalent to the LaGrange multipliers, can be approximated by using

$$\{F_c\} = [C]^T[\alpha][C]\{\delta\} \tag{12}$$

Penalty Parameters

The $[\alpha]$ matrix in the triple matrix product $[C]^T[\alpha][C]$ is a 3×3 matrix containing the penalty parameters on the diagonal and zeroes elsewhere. To add flexibility to the formulation, three penalty parameters are specified: two that maintain continuity of the interlaminar shear stresses through the thickness and a third that maintains continuity of the interlaminar normal stress through the thickness. Specifically, these are referred to as $(\alpha_u, \alpha_v, \alpha_w)$, where the subscript identifies the appropriate continuity through the thickness. There exist situations where there is continuity in the interlaminar normal stress through the thickness, but discontinuity in the interlam-

inar shear stresses, as in a delamination that is being compressed. The present formulation allows for this by preventing two layers from displacing through each other in the z direction. The penalty parameters α_u and α_v are set equal to zero and α_w is set equal to a very large number. This creates a discontinuity in the transverse shear stresses but maintains continuity through the thickness for the transverse normal stress.

III. Stress Analysis

Constitutive Equations

Stresses computed by using the constitutive equations for the 20-noded element proceed directly from the displacements. Utilizing the three-dimensional, triquadratic shape functions of the 20-noded solid element, Eqs. (1-3) show that each of the three displacements is quadratic with respect to each of the coordinates x, y, and z. The strains, which are partial derivatives of the displacements, are given as

$$\epsilon_x = \frac{\partial u}{\partial x} \Rightarrow \epsilon_x = h_1(x,y^2,z^2) \tag{13}$$

$$\epsilon_y = \frac{\partial v}{\partial y} \Rightarrow \epsilon_y = h_2(x^2,y,z^2) \tag{14}$$

$$\epsilon_z = \frac{\partial w}{\partial z} \Rightarrow \epsilon_z = h_3(x^2,y^2,z) \tag{15}$$

$$\gamma_{xy} = \frac{\partial u}{\partial y} + \frac{\partial v}{\partial x} \Rightarrow \gamma_{xy} = h_4(x^2,y^2,z^2) \tag{16}$$

$$\gamma_{xz} = \frac{\partial u}{\partial z} + \frac{\partial w}{\partial x} \Rightarrow \gamma_{xz} = h_5(x^2,y^2,z^2) \tag{17}$$

$$\gamma_{yz} = \frac{\partial v}{\partial z} + \frac{\partial w}{\partial y} \Rightarrow \gamma_{yz} = h_6(x^2,y^2,z^2) \tag{18}$$

The variation with respect to the through the thickness coordinate z of the shear strains is quadratic. In matrix form, the calculation of the strains for layer k is

$$\{\epsilon\}^k = [B]^k\{\delta\}^k \tag{19}$$

The stresses in layer k are computed using the three-dimensional stress-strain relations, which are expressed in matrix notation as

$$\{\sigma\}^k = [D]^k\{\epsilon\}^k \tag{20}$$

Because of the variations in the strains indicated by Eqs. (13-18), the stresses, as computed in Eq. (20), vary quadratically in all three directions. Using the 20-noded element allows for computation of the σ_z from the constitutive equations—a significant advantage over the plate element—but at the cost of more degrees of freedom and bigger models. Another significant departure from the plate element is that the interlaminar shear stresses computed from the constitutive equations for the solid element vary quadratically through the thickness. Determining whether there is any benefit to integrating the equilibrium equations is the next task.

Equilibrium Equations

Integrating the equilibrium equations through the thickness results in a much improved parabolic distribution of interlaminar shear stresses through the thickness of the 20-noded solid element. As shown earlier, the stresses computed using the constitutive equations vary quadratically in all three directions. Neglecting body forces, the equilibrium equations are expressed as

$$\frac{\partial \sigma_x}{\partial x} + \frac{\partial \tau_{xy}}{\partial y} + \frac{\partial \tau_{xz}}{\partial z} = 0 \tag{21}$$

$$\frac{\partial \tau_{xy}}{\partial x} + \frac{\partial \sigma_y}{\partial y} + \frac{\partial \tau_{yz}}{\partial z} = 0 \tag{22}$$

$$\frac{\partial \tau_{xz}}{\partial x} + \frac{\partial \tau_{yz}}{\partial y} + \frac{\partial \sigma_z}{\partial z} = 0 \tag{23}$$

Rearranging the equilibrium equations to solve for the through the thickness stresses yields

$$\frac{\partial \tau_{xz}}{\partial z} = -\left(\frac{\partial \sigma_x}{\partial x} + \frac{\partial \tau_{xy}}{\partial y}\right) \Rightarrow \tau_{xz} = p_1(x^2,y^2,z^3) \tag{24}$$

$$\frac{\partial \tau_{yz}}{\partial z} = -\left(\frac{\partial \tau_{xy}}{\partial x} + \frac{\partial \sigma_y}{\partial y}\right) \Rightarrow \tau_{yz} = p_2(x^2,y^2,z^3) \tag{25}$$

Solving for the interlaminar shear stresses by integrating Eqs. (24) and (25) provides the improved cubic variation in the z direction illustrated by the functional forms in Eqs. (24) and (25).

Computing the partial derivatives of the equilibrium equations relies on the smoothing functions derived for the in-plane stresses. The smoothing functions are based on the values of the in-plane stresses at the Gauss points. Cook[7] documents that, for the quadratic solid element, the location of the optimal points for stress calculation are the $2 \times 2 \times 2$ Gauss points. Since stresses are computed for each layer for the solid element in the present work, Gauss points in the transverse direction are not used. A detailed investigation was undertaken to determine the optimal points of stress calculation, and the results verified that the 2×2 points were optimal for stress calculation. With only four points of stress calculation, bilinear smoothing functions of the form

$$\sigma_x = C_0 + C_1\xi + C_2\eta + C_c\xi\eta \tag{26}$$

are derived for the in-plane stresses. The biquadratic variance through the thickness of the in-plane stresses is implicit to the formulation.

Partial derivatives with respect to the ξ and η of the in-plane stresses are easily computed for each layer from the smoothing functions, and the inverse of the Jacobian matrix is used to transform them to partial derivatives with respect to x and y. Equations (24) and (25) can be rewritten for the jth layer as

$$\Delta\tau_{xz_j} = -\left(\frac{\partial \sigma_x}{\partial x} + \frac{\partial \tau_{xy}}{\partial y}\right)_j \Delta z_j \tag{27}$$

$$\Delta\tau_{yz_j} = -\left(\frac{\partial \tau_{xy}}{\partial x} + \frac{\partial \sigma_y}{\partial y}\right)_j \Delta z_j \tag{28}$$

where $\Delta\tau_{ij}$ represents the change in stress from the lower to the upper surface of layer j and Δz_j is the thickness of layer j. The right-hand sides of Eqs. (27) and (28) are known based on the derivatives of the smoothing functions for layer j and the thicknesses; hence, shortening the right-hand sides, equation (27), expressed for the jth layer, becomes

$$\tau_{xz_{j+1}} - \tau_{xz_j} = I_{xz_j} \tag{29}$$

For a laminate that is continuous through the thickness, the lower and upper surfaces are shear-free surfaces. Writing Eq. (29) in matrix notation for n layers yields

$$\begin{bmatrix} 1 & 0 & \cdots & \cdots & \cdots & 0 \\ -1 & 1 & 0 & \cdots & \cdots & 0 \\ 0 & -1 & 1 & \cdots & \cdots & 0 \\ \vdots & \ddots & \ddots & \ddots & \ddots & \vdots \\ 0 & \cdots & \cdots & \cdots & -1 & 1 \\ 0 & 0 & 0 & \cdots & 0 & -1 \end{bmatrix} \begin{bmatrix} \tau_{xz_2} \\ \vdots \\ \vdots \\ \vdots \\ \vdots \\ \tau_{xz_n} \end{bmatrix} = \begin{bmatrix} I_{xz_1} \\ \vdots \\ \vdots \\ \vdots \\ \vdots \\ I_{xz_n} \end{bmatrix} \tag{30}$$

Table 1 Normalized stresses in a [0 deg/90 deg/0 deg] square simply supported plate subjected to a sinusoidally varying pressure

S	Layers	$\bar{\sigma}_x$ $(\frac{a}{2},\frac{a}{2},\pm\frac{h}{2})$	$\bar{\sigma}_y$ $(\frac{a}{2},\frac{a}{2},\pm\frac{h}{6})$	$\bar{\tau}_{xy}$ $(0,0,\pm\frac{h}{2})$	$\bar{\tau}_{xz}$ $(0,\frac{a}{2},0)$ Constitutive	$\bar{\tau}_{xz}$ $(0,\frac{a}{2},0)$ Equilibrium	$\bar{\tau}_{yz}$ $(\frac{a}{6},0,0)$ Constitutive	$\bar{\tau}_{yz}(\frac{a}{6},0,0)$ Equilibrium
	1	0.454	0.355	0.045	0.155	0.298	0.142	0.196
	3	0.750	0.545	0.064	0.354	0.262	0.223	0.244
4	5	0.761	0.548	0.064	0.375	0.325	0.228	0.239
	E	0.755	0.556	0.051	0.282	0.282	0.217	0.217

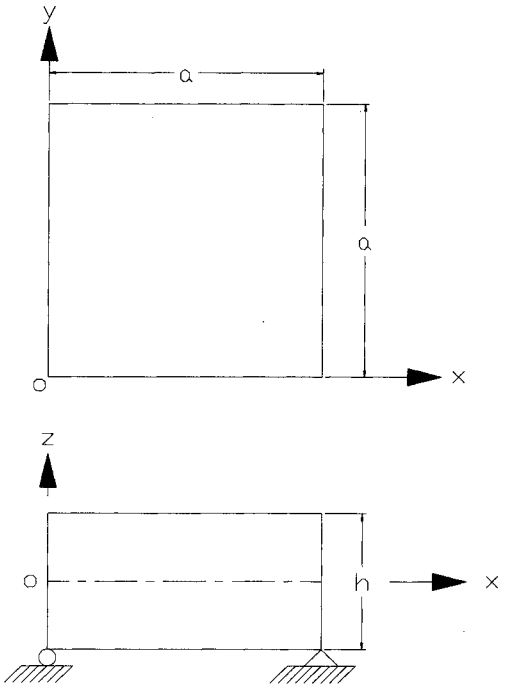

Fig. 3 Notation for the simply supported square [0 deg/90 deg/0 deg] plate subjected to a transverse sinusoidal distributed pressure.

Equation (30) represents n equations in $n-1$ unknown interlaminar shear stresses at the layer interfaces. Utilizing a least squares orthonormalization procedure, Eq. (30) is solved for the shear stresses at the layer interfaces. This procedure is similarly performed to solve for τ_{yz} at the layer interfaces as well. Computing the interlaminar normal stress from equilibrium, however, is not beneficial. Creating bilinear smoothing functions for the interlaminar shear stresses from equilibrium and integrating gives

$$\frac{\partial \sigma_z}{\partial z} = -\left(\frac{\partial \tau_{xz}}{\partial x} + \frac{\partial \tau_{yz}}{\partial y}\right) \Rightarrow \sigma_z = p_3(x^2, y^2, z^2) \tag{31}$$

Since there is no benefit from computing the transverse normal stress from the equilibrium equations, all transverse normal stress results presented herein are computed using the constitutive equations.

IV. Results

Sinusoidal Bending Stresses

The effect of transverse shear deformation and the inadequacies of classical laminated plate theory (CPT) were demonstrated by Pagano[8] in 1970. He derived exact elasticity solutions for square and rectangular bidirectional plates subjected to a sinusoidally varying transverse pressure. Comparisons to CPT showed the significance of transverse shear deformation, particularly for plates with low span-to-depth ratios. He notes that two of the limitations of CPT are the restriction of the Kirchhoff hypothesis, which, by forcing normals to remain normal, neglects shear deformation and the use of a plane stress constitutive law, which poorly characterizes the interlaminar stresses. As the span-to-depth ratio increases, CPT converges to the elasticity solution. Two of these cases discussed by Pagano are considered in the present work.

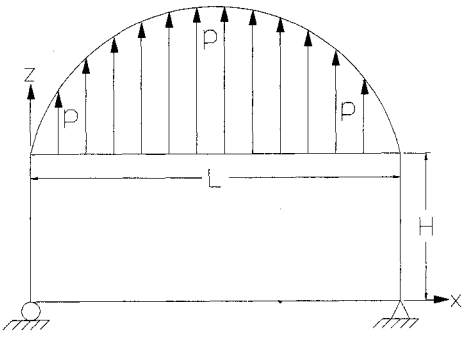

Fig. 4 Reference coordinate system for the model of the plate strip subjected to cylindrical bending.

The sinusoidal variation of the pressure is given by

$$p = q_0 \sin\frac{\pi x}{a} \sin\frac{\pi y}{a} \tag{32}$$

Consistent nodal forces are computed using

$$\{F_i\} = -\int_A [N_i]^T p \, dA \tag{33}$$

where

$$\{F_i\}^T = [F_{x_i} \; F_{y_i} \; F_{z_i}] \tag{34}$$

and $[N_i]$ is a matrix consisting of the shape functions.

The first case modeled is a square plate with dimensions $a \times a$ and of thickness h. Figure 3 shows the geometry and the boundary conditions of the problem, and a uniform 6×6 mesh is used with the number of layers through the thickness varying from 1 to 5. The orthotropic material properties of the plate are those typical for a high modulus graphite epoxy: $E_L/E_T = 25$, $G_{LT}/G_{TT} = 2.5$, and $\nu_{LT} = \nu_{TT} = 0.25$, where L indicates the direction parallel to the fibers, and T is perpendicular to the fibers. Table 1 presents normalized stresses for a simply supported square [0 deg/90 deg/0 deg] plate subjected to a sinusoidally varying load using the 20-noded solid element for a span-to-depth (aspect) ratio of four. In-plane stresses are computed using the constitutive equations, while the interlaminar shear stresses are found by integrating the equilibrium equations. The normalized quantities are

$$(\bar{\sigma}_x, \bar{\sigma}_y, \bar{\tau}_{xy}) = \frac{1}{q_0 S^2}(\sigma_x, \sigma_y, \tau_{xy}) \tag{35}$$

$$(\bar{\tau}_{xz}, \bar{\tau}_{yz}) = \frac{1}{q_0 S}(\tau_{xz}, \tau_{yz}) \tag{36}$$

where q_0 is the maximum pressure, applied at the center of the plate, and S is the aspect ratio. All values of stresses represent maximum values, and the table indicates the points of consideration on the plate. Refer to Fig. 3 to locate those points on

the plate. For an aspect ratio of 4, significant improvement is achieved as the layers are increased from 1 to 5. The solution labelled E represents the exact elasticity solution derived by Pagano.[8] Interlaminar shear stresses from both constitutive and equilibrium equations are included. As discussed earlier, interlaminar shear stresses computed from constitutive equations are quadratic through the thickness, whereas those stresses computed using equilibrium equations are cubic through the thickness. Close observation of Table 1 shows that interlaminar shear stresses found by integrating the equilibrium equations are clearly more accurate than those computed from the constitutive equations.

Cylindrical Bending Stresses

A second example considered is the cylindrical bending of cross-ply composite plates with aspect ratios of 4. In 1969, Pagano[9] provided exact elasticity solutions for the cylindrical bending of a [0 deg/90 deg/0 deg] orthotropic plate. Again, his solutions demonstrated the deficiencies of CPT. Figure 4 shows the coordinate system of the model. Because of the simplicity of the loading and boundary conditions, only a strip of elements is required to effectively model the cylindrical bending problem. The orthotropic material properties are identical to those in the previous example. The following figures present plots of normalized in-plane normal stress and interlaminar shear stress through the thickness of the plate strip. The functions are normalized as follows

$$\bar{\tau}_{xz} = \frac{\tau_{xz}(0, z)}{q_0}; \qquad \bar{z} = \frac{z}{H} \tag{37}$$

where q_0 is the maximum applied pressure, which occurs at the center of the plate strip, H the total thickness of the plate strip, L the total length of the strip, and E_T the elastic modulus transverse to the fiber direction. For the finite element results,

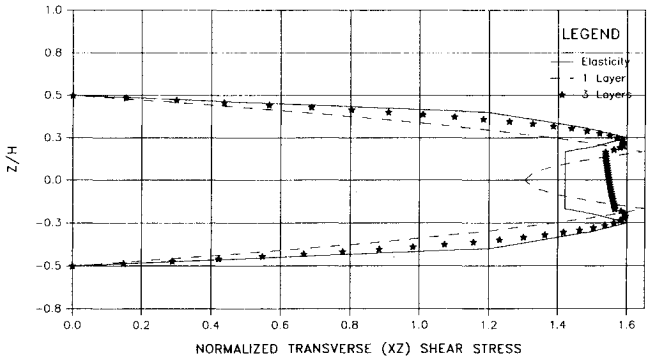

Fig. 5 Normalized interlaminar shear stress through the thickness for a [0 deg/90 deg/0 deg] plate subjected to cylindrical bending.

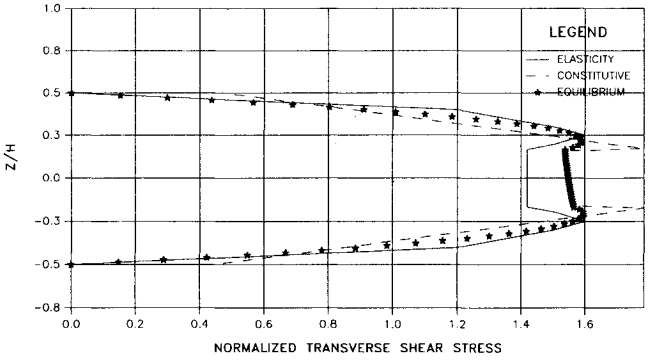

Fig. 6 Comparison between computation of the interlaminar shear stresses with the constitutive equations and the equilibrium equations.

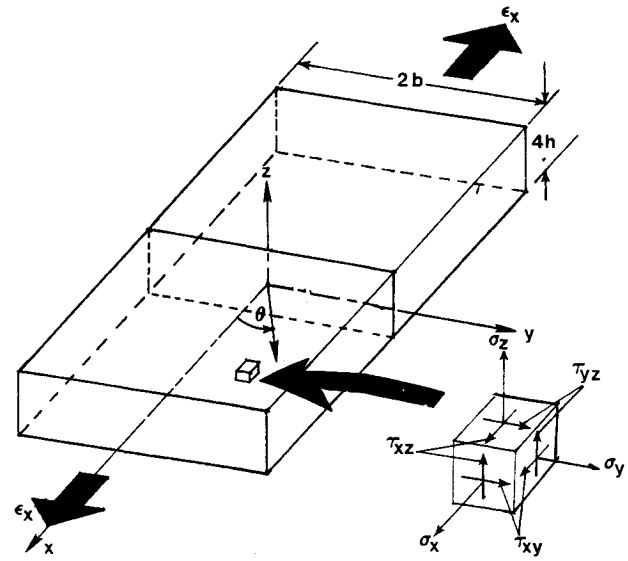

Fig. 7 Geometry and notation for composite laminated plate subjected to a uniform axial load in the x direction.

a 20-element strip of uniform elements is used in the plane, and models containing 1 and 3 layers are used through the thickness. The transverse pressure for cylindrical bending is given by

$$p = q_0 \sin \frac{\pi x}{L} \tag{38}$$

where q_0 is the applied pressure, and L is the length of the strip. To compute the consistent nodal forces, the pressure is integrated over area as in Eq. (33).

The first case considered is the cylindrical bending of a cross-ply [0 deg/90 deg/0 deg] simply supported plate strip of span-to-depth ratio equal to 4. Figure 5 shows the interlaminar shear stress τ_{xz} between the [0 deg/90 deg] layers through the thickness of the laminate. Both one- and three-layer models are compared to the exact elasticity solution and the plotted interlaminar shear stresses were found by integrating the equilibrium equations. Significant improvement with additional layers is clearly in evidence. A comparison of interlaminar shear stresses computed with the constitutive equations and those calculated by integrating the equilibrium equations for a three-layer model is shown in Fig. 6. As with the previous example, the integration of the equilibrium equations has improved the interlaminar shear stress predictions for the 20-noded solid element. It is notable at this point that Fuehne[10] introduced a detailed comparison of interlaminar shear stresses computed with the constitutive equations and the equilibrium equations in thick composite plates with both the 20-noded solid element and the eight-noded plate element. For both of the cases considered in this paper, the eight-noded plate element penalty formulation provided more accurate interlaminar shear stresses than the 20-noded element formulation. This is a significant conclusion as the eight-noded plate element, with 48 degrees of freedom per element, is more computationally efficient than the 20-noded solid element with 60 degrees of freedom per element. As mentioned earlier, though, the eight-noded plate element is incapable of modeling problems with significant interlaminar normal stresses. One of those examples is the free-edge problem.

Free-Edge Stresses in Cross-Ply Laminates

In 1970, Pipes and Pagano[11] studied the stress field near a free edge in a symmetric composite laminate subjected to a uniform in-plane strain. For an isotropic or unidirectional composite laminate, these stresses do not exist. However, when composite layers of different fiber orientation are

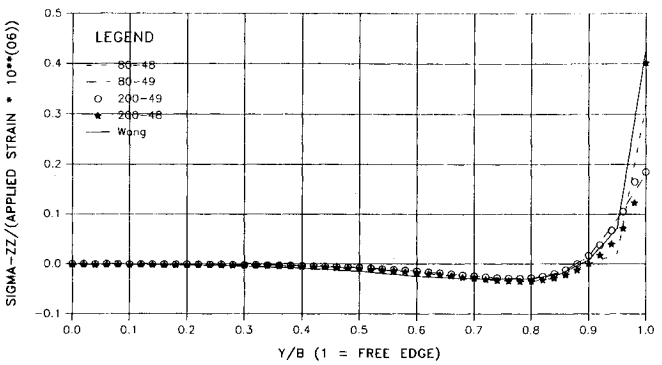

Fig. 8 Transverse normal stress between the [0 deg/90 deg] layers of a [0 deg/90 deg]$_S$ laminate subjected to axial extension.

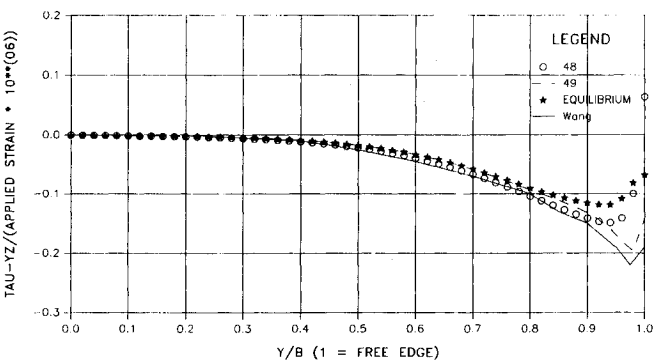

Fig. 9 Interlaminar shear stress between the [0 deg/90 deg] layers of a [0 deg/90 deg]$_S$ laminate subjected to axial extension. Fifty uniform elements are used from the center to free edge of the plate.

stacked in a laminate, the resulting mismatch in Poisson's ratio creates a complicated elastic response. Complex shear-transfer mechanisms between layers produce significant transverse shear and normal stresses between layers, which adversely affect the strength and life of a composite. Using a finite difference solution of the elastic equations, they suggested the possibility of a stress singularity at the free edge.

In 1976, Wang and Crossman[12] adapted the skyline matrix storage scheme and, together with a constant strain triangular finite element formulation, developed a two-dimensional solution that reinforced the singularity proposal. Their published solution represents a benchmark for the free-edge problem. In the following examples, interlaminar normal stress is computed by employing the constitutive equations while the interlaminar shear stresses are found both by utilizing the constitutive equations and by integrating the equilibrium equations.

The first case considered is the uniform axial extension of a [0 deg/90 deg]$_S$ laminate. Figure 7 shows the geometry and notation of the free-edge problem. Note that the fiber orientation angle θ is defined with respect to the x axis, the direction of the applied strain. For the [0 deg/90 deg]$_S$ laminate, two four-layer models consisting, respectively, of a strip of 20 and 50 uniformly spaced 20-noded elements per layer were used. Consistent nodal forces for a laminate subjected to a uniform axial strain are found by using

$$\{F\} = \sum_{k=1}^{NL} \left(\int_{-1}^{+1} \int_{-1}^{+1} [B]^{kT}[D]^k \{\epsilon_0\} \|J\|^k \, d\xi \, d\eta \right) \qquad (39)$$

where $\{F\}$ is the vector of elemental nodal forces, ϵ_0 the applied strain, $[B]$ the strain-displacement matrix, $[D]$ the stress-strain matrix, NL the number of plies, $\|J\|$ the determinant of the Jacobian matrix, and ξ and η the isoparametric coordinates. The two-dimensional integral is evaluated using (3 × 3) Gauss integration.

Figure 8 compares the transverse normal stress σ_z, computed using the constitutive equations, between the [0 deg/90 deg] layers of the laminate, with the results derived by Wang and Crossman. The smaller model has 20 elements per layer and the larger has 50 elements per layer. The elements are uniformly spaced from the center of the plate to the free edge. Since each model contains four layers, the smaller model has 80 elements and the larger model has 200 elements. Note that the model size is indicated in the legend. The present results compare favorably with Wang and Crossman's results, and note that the finer mesh produced little improvement. The 48 and 49 labels in the legend refer to the sublayer, or ply, from which the stress values are obtained. As previously described, the stresses from the constitutive relations are computed for each ply. Typically, each layer is subdivided into 24 plies, and 24 would be the value of NL in Eqs. (5) and (39). As a result, the stresses from the constitutive equations are not at the interface but at the center of the plies. In these four-layer models, therefore, there are 96 plies in which stresses are computed and 48 and 49 represent the values at the center of the plies on either side of the interface. Careful inspection of Fig. 8 shows that there can be a nontrivial difference between the values on either side of the interface. A recommendation for determining the value of the stress at the interface is to average the values on either side of the interface. This is also true for the interlaminar shear stresses presented in the forthcoming figures.

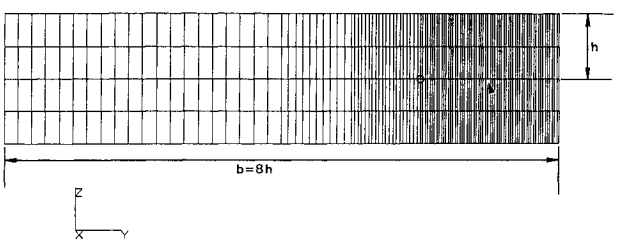

Fig. 10 Side view of the model of a [0 deg/90 deg]$_S$ laminate with a debond between the [0 deg/90 deg] interface, which is indicated by the arrow. The layer thickness is h and the circle marks the distance $2h$ from the free edge.

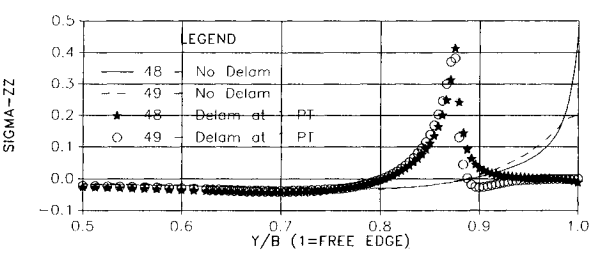

Fig. 11 Transverse normal stress σ_z between the [0 deg/90 deg] layers of a [0 deg/90 deg]$_S$ laminate subjected to axial extension with a delamination at the free edge equal to one ply thickness.

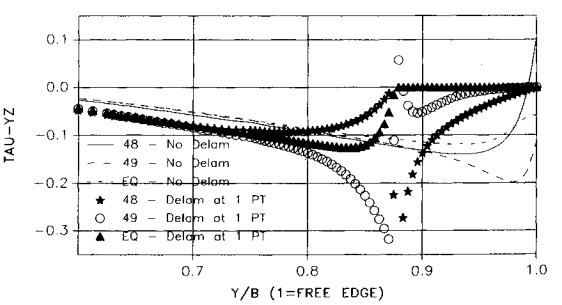

Fig. 12 Interlaminar shear stress τ_{yz} between the [0 deg/90 deg] layers of a [0 deg/90 deg]$_S$ laminate subjected to axial extension with a delamination at the free edge equal to one ply thickness.

Figure 9 contains interlaminar shear stresses between the [0 deg/90 deg] layers for the same $[0 \text{ deg}/90 \text{ deg}]_S$ laminate subjected to axial extension. The model has four layers with 50 uniformly spaced elements per layer. Of particular interest is the comparison between interlaminar shear stresses computed with the constitutive and equilibrium equations. In the legend, the curves labeled 48 and 49 represent stresses computed using the constitutive equations in the sublayers on either side of the interface. The stresses calculated with the equilibrium equations are located at the interface, as are Wang and Crossman's data, and depict a more realistic solution as a result. For this problem, the free edge is a stress-free surface and, from Fig. 9, it's notable that shear stresses computed by integrating the equilibrium equations best approximate this condition.

Stresses near a Free-Edge Debond

As previously mentioned, the penalty function formulation described herein allows stress analysis of problems with discontinuities through the thickness. Although there are no available solutions with which to compare, a cross-ply, $[0 \text{ deg}/90 \text{ deg}]_S$ plate with a delamination between the [0 deg/90 deg] layers at the free edge and subjected to a uniform axial strain is considered. The notation and geometry for this problem are given by Fig. 7. Three different debond lengths, including one-half, one, and two ply thicknesses from the free edge, are examined in detail by Fuehne.[10] In this work, only the debond length equal to one ply thickness is presented. A model, consisting of four layers and 110 20-noded elements per layer, is displayed in Fig. 10. Note that the debond lies between the second and third layer, as indicated by the arrow, and that the circle is a distance $2h$ away from the free edge. Through the skillful use of PATRAN,[13] a model limiting the use of the penalty functions to certain predetermined critical interfaces is created. In this model, penalty functions are only used for the distance between the circle and the free edge. Varying debond lengths are obtained by setting the penalty parameters (analogous to spring constants) equal to either a large number, representing continuity, or zero, signifying discontinuity. Because of the flexibility of the formulation, models with relatively small bandwidths and storage requirements are possible.

Figure 11 presents the transverse normal stress between the [0 deg/90 deg] layers for free-edge debond thicknesses equal to one thickness along with the stresses obtained earlier for the free-edge problem with no debond. Similarly, the curves labeled 48 and 49 refer to the plies located on either side of the [0 deg/90 deg] interface. All transverse normal stress values are computed using the constitutive equations. A significant stress magnification, nearly equal to that at the free edge without the debond, is realized at the tip of the debond. It is notable that the area between the debond crack front and the free edge is a stress-free surface. Averaging the interlaminar normal stresses on either side of the interface produces a value very near zero.

Finally, Fig. 12 reveals the predicted interlaminar shear stress field near the debond between the [0 deg/90 deg] layers. Again, designations 48 and 49 refer to interlaminar shear stresses computed using the constitutive equations on either side of the interface. Interlaminar shear stresses calculated by integrating the equilibrium equations are labeled as EQ. Again, a significant shear-stress magnification, which approaches twice that of the bonded free-edge value, is observed at the tip of the debond. Close examination of the plot indicates that averaging the interlaminar shear stresses computed using the constitutive equations produces a value approximately equal to those found by integrating the equilibrium equations everywhere except for a short distance near the debond tip and the area beyond the tip. A very important observation is that the free surface between the debond front and the free edge is a shear-free surface. The integration of the equilibrium equations automatically produces zero interlaminar shear stress at those interfaces. The interlaminar shear stresses computed by employing the constitutive equations, however, are not zero on either side of the interface and even an average of the values above and below the interface does not produce zero stress. Obviously, the interlaminar shear stresses calculated by integrating the equilibrium equations are more realistic than those from the constitutive equations for this problem.

V. Conclusions and Recommendations

In this work, a unique coupling of a 20-noded solid element formulation, the integration of the equilibrium equations, and a penalty function method are detailed. Interlaminar shear-stress predictions through the thickness are improved by integrating the equilibrium equations for thick laminated plates and a cross-ply plate subjected to a uniformly applied strain. By using the penalty functions to represent discontinuity between layers, interlaminar normal and shear stresses are investigated in a cross-ply plate with a debond at the free edge and subjected to a uniform strain. Significant magnifications in interlaminar normal and shear stress occur at the tip of the debond. A more suitable variation of interlaminar shear stresses is obtained for the debond problem by integrating the equilibrium equations through a stack of elements and accounting for the discontinuity at the debond. The forces of constraint between nodes may be approximated using the nodal displacements with the penalty functions. In this work, the forces of constraint are not utilized; however, these forces could be utilized in a fracture mechanics approach to estimate debond growth.

References

[1]Engblom, J. J., Fuehne, J. P., and Hamdallah, J. M., "Transverse Stress Calculations for Laminated Composite Shell Structures Using Plate/Shell Finite Element Formulations," *Journal of Reinforced Plastics and Composites,* Vol. 8, No. 5, 1989, pp. 446–457.

[2]Engblom, J. J., and Ochoa, O. O., "Finite Element Formulation Including Interlaminar Stress Calculations," *Computers & Structures,* Vol. 23, No. 2, 1986, pp. 241–249.

[3]Engblom, J. J., and Fuehne, J. P., "Transverse Stress Predictions for Thin-to-Thick Composite Structures: Shear Deformable Finite Element Penalty Formulation," *Proceedings of 5th International Conference on Composite Structures,* Elsevier Applied Science, London, July, 1989.

[4]Fuehne, J. P., and Engblom, J. J., "A Shear Deformable Finite Element Penalty Formulation for Predicting Transverse Stresses in Thick Composite Structures," *Proceedings of ASC 4th Technical Conference on Composite Materials,* Technomic, Lancaster, PA, 1989.

[5]Chatterjee, S. N., and Ramnath, V., "Modeling Laminated Composite Structures as Assemblage of Sublaminates," *International Journal of Solids and Structures,* Vol. 24, No. 5, 1988, pp. 439–458.

[6]Chatterjee, S. N., "Three- and Two-Dimensional Stress Fields Near Delaminations in Laminated Composite Plates," *International Journal of Solids and Structures,* Vol. 23, No. 4, 1987, pp. 1535–1548.

[7]Cook, R. D., *Concepts and Applications of Finite Element Dialysis,* 2nd ed., Wiley, New York, 1981, pp. 271–301.

[8]Pagano, N. J., "Exact Solutions for Rectangular Bidirectional Composites and Sandwich Plates," *Journal of Composite Materials,* Vol. 4, No. 1, 1970, pp. 20–34.

[9]Pagano, N. J., "Exact Solutions for Composite Laminates in Cylindrical Bending," *Journal of Composite Materials,* Vol. 3, No. 7, 1969, pp. 398–411.

[10]Fuehne, J. P., "A Finite Element Method Including Transverse Stresses for Thick Laminated Plates and Shells," Ph.D. Dissertation, Mechanical Engineering Dept., Texas A&M Univ., College Station, TX, Dec. 1991.

[11]Pipes, R. B., and Pagano, N. J., "Interlaminar Stresses in Composite Laminates Under Uniform Axial Extension," *Journal of Composite Materials,* Vol. 4, No. 10, 1970, pp. 538–548.

[12]Wang, A. S. D., and Crossman, F. W., "Some New Results on Edge Effect in Symmetric Composite Laminates," *Journal of Composite Materials,* Vol. 11, No. 1, 1977, pp. 92–106.

[13]Kramer, D. M. (ed.), "PATRAN Plus," PATRAN Division of PDA Engineering, Costa Mesa, CA, 1989.